Human Molecular Genetics, 2011, Vol. 20, No. 8 **1536–1546**
doi:10.1093/hmg/ddr031
Advance Access published on January 24, 2011

Over-expression of *Grhl2* causes spina bifida in the *Axial defects* mutant mouse

Madeleine R. Brouns[1,†], Sandra C.P. De Castro[4], Els A. Terwindt-Rouwenhorst[1], Valentina Massa[4,‡], Johan W. Hekking[1], Caroline S. Hirst[4], Dawn Savery[4], Chantal Munts[1], Darren Partridge[4], Wout Lamers[1,2], Eleonore Köhler[1,2], Henny W. van Straaten[1,3], Andrew J. Copp[4] and Nicholas D.E. Greene[4,*]

[1]Department of Anatomy and Embryology, [2]Research School NUTRIM and [3]Research School GROW, Maastricht University Medical Center, University of Maastricht, PO Box 616, 6200 MD, Maastricht, The Netherlands and [4]Neural Development Unit, UCL Institute of Child Health, London WC1N 1EH, UK

Received December 14, 2010; Revised and Accepted January 19, 2011

Cranial neural tube defects (NTDs) occur in mice carrying mutant alleles of many different genes, whereas isolated spinal NTDs (spina bifida) occur in fewer models, despite being common human birth defects. Spina bifida occurs at high frequency in the *Axial defects* (*Axd*) mouse mutant but the causative gene is not known. In the current study, the *Axd* mutation was mapped by linkage analysis. Within the critical genomic region, sequencing did not reveal a coding mutation whereas expression analysis demonstrated significant up-regulation of *grainyhead-like 2* (*Grhl2*) in *Axd* mutant embryos. Expression of other candidate genes did not differ between genotypes. In order to test the hypothesis that over-expression of *Grhl2* causes *Axd* NTDs, we performed a genetic cross to reduce *Grhl2* function in *Axd* heterozygotes. *Grhl2* loss of function mutant mice were generated and displayed both cranial and spinal NTDs. Compound heterozygotes carrying both loss (*Grhl2* null) and putative gain of function (*Axd*) alleles exhibited normalization of spinal neural tube closure compared with *Axd*/+ littermates, which exhibit delayed closure. *Grhl2* is expressed in the surface ectoderm and hindgut endoderm in the spinal region, overlapping with *grainyhead-like 3* (*Grhl3*). *Axd* mutants display delayed eyelid closure, as reported in *Grhl3* null embryos. Moreover, *Axd* mutant embryos exhibited increased ventral curvature of the spinal region and reduced proliferation in the hindgut, reminiscent of *curly tail* embryos, which carry a hypomorphic allele of *Grhl3.* Overall, our data suggest that defects in *Axd* mutant embryos result from over-expression of *Grhl2*.

INTRODUCTION

Formation of the neural tube in higher vertebrates depends on elevation, folding, apposition and fusion of the neural folds, a process known as primary neurulation (1,2). Failure of this process results in open neural tube defects (NTDs), which are among the most common congenital malformations in humans (3). Although there is strong evidence for a genetic component in NTDs, identification of the causative genes is complicated by the fact that most cases appear to involve a combination of genetic and environmental factors (4,5). The large number of mouse genetic models in which NTDs arise as part of the phenotype emphasize the possible genetic complexity of these defects and provide insight into the multiple molecular requirements for neural tube closure (3,6,7).

*To whom correspondence should be addressed at: Neural Development Unit, UCL Institute of Child Health, 30 Guilford Street, London WC1N 1EH, UK. Tel: +44 2079052217; Email: n.greene@ich.ucl.ac.uk
†Present address: Department of Health and Life Sciences, VU University Amsterdam, De Boelelaan 1085, 1081 HV, Amsterdam, The Netherlands.
‡Present address: University of Milano-Bicocca, Department of Pediatrics, Hospital S.Gerardo/Fondazione MBBM, Via Pergolesi, 3320052 Monza, Italy.

In humans, cranial NTDs (anencephaly) and caudal NTDs (spina bifida) occur at approximately equal frequency (8,9). By comparison, a survey of the various NTD mutants in mice reveals a striking predominance of models in which cranial NTDs occur. Thus, exencephaly occurs in isolation (~75% of mutants) or in combination with spina bifida (~20% of mutants) in most models (7). In contrast, isolated spina bifida is observed in only ~5% of the roughly 250 mouse NTD mutants. Among NTDs induced by various teratogens, exencephaly is also induced more frequently than spina bifida (10). Thus, cranial neural tube closure appears exquisitely sensitive to disruption in mice. It may be that cranial neural tube closure in the mouse embryo is more complex than in humans, requiring coordinated function of many gene products. Hence, there is a relative paucity of mouse models for isolated spinal NTDs, despite the importance of these malformations in humans.

The *Axial defects* (*Axd*) mutation arose spontaneously in the 1980s and was recognized on the basis of a curled tail phenotype inherited as a semi-dominant Mendelian trait (11). The penetrance of tail defects among *Axd*/+ mice varies with genetic background, being highest on the BALB/c background with ~50–60% of mice affected (12). Intercrosses of heterozygotes produced litters containing neonates with spina bifida, presumed to be homozygous mutants (11). At embryonic day (E) 12.5, ~25% of embryos showed spina bifida, suggesting that spinal NTDs are fully penetrant among homozygotes at this stage (12). Cranial NTDs were not observed. Among neonates, there was a lower incidence of curled tails and spina bifida than expected. This was suggested to indicate possible correction of tail defects and/or soft tissue healing over open lesions during late gestation (11,12). However, inability to genotype litters precluded further analysis of this possibility.

In the current study, we mapped the *Axd* mutation to a region of chromosome 15 containing the *grainyhead-like 2* (*Grhl2*) gene, which encodes a transcription factor. We found that loss of function of *Grhl2* causes cranial and spinal NTDs, as previously observed for *Grhl3* mutants (13–15). Expression analysis in *Axd* mutant embryos showed over-expression of *Grhl2*, whereas reduction of *Grhl2* expression levels resulted in normalization of spinal neural tube closure. We conclude that both insufficient and excessive expression of *Grhl2* can cause NTDs.

RESULTS

Axial defects mutant embryos display severe spina bifida

The phenotype of embryos among litters from *Axd*/+ intercrosses was examined by scanning electron microscopy (70 embryos) and light microscopy (>300 embryos), at developmental stages during and after the stage of spinal neural tube closure (E9.5–10.5 and later). Initial studies were performed prior to linkage analysis, with the prediction that embryos exhibiting failure of neural tube closure would correspond to homozygous mutant embryos. These phenotype–genotype correlations were confirmed following mapping of the *Axd* mutation (see what follows). Abnormalities in spinal neural tube closure could be detected from around the 24 somite stage (E9.5), when homozygous *Axd/Axd* embryos exhibited an enlarged posterior neuropore (PNP) compared with wild-type littermates (Fig. 1A and B). The PNP (the final region of open spinal neural folds) is very small or closed by the 31–32 somite stage (E10.5) in wild-type embryos (Figs 1C and E, and 2C), whereas homozygous mutants display very large open PNPs, of up to 3 mm in length (Figs 1D and F, and 2C). The rostral limit of the open PNP was at the level of somites 22–26, indicating that closure had failed to progress beyond this axial level.

Examination of embryos at more advanced somite stages, at E10.5 and E11.5, showed that the PNP of *Axd* mutants did not reduce in size but remained persistently open. This defect corresponds to spina bifida, which can be readily visualized in affected fetuses as a typical protrusion of tissue from the open lesion at E16.5 (Fig. 1G). Transverse sections at the level of the lesion reveal the degeneration of spinal cord tissue (Supplementary Material, Fig. S1C and D). Damage appears most severe at the sacral level where none of the typical architecture of the neural tube can be discerned, whereas motor neurons are still detectable in the lumbar region (Supplementary Material, Fig. S1A and B). By birth, the exposed nervous tissue has degenerated and the open vertebral arches are exposed at the dorsal surface (Supplementary Material, Fig. S1E). Some fetuses with spina bifida at E16.5 and 17.5 exhibit a 'remnant' of the tail which we hypothesize to result from apparent degeneration of the tail (Supplementary Material, Fig. S2D).

In the majority of heterozygous *Axd*/+ embryos, closure of the PNP was complete by the 35 somite stage or soon after (Fig. 2C). This reflects a delay in closure compared with wild-type embryos, apparent as a higher mean PNP length in heterozygotes than wild-type littermates at the 26–28, 29–31 and 32–34 somite stages ($P < 0.001$). Delayed PNP closure manifests at later stages as a tail flexion defect or 'curly tail' in ~40–50% of *Axd*/+ mice on the BALB/c background.

The Axd mutation maps to proximal chromosome 15

In order to map the mutation underlying the *Axd* phenotype, a congenic strain was first generated on the BALB/c genetic background, selected for high penetrance of the dominant (heterozygous) phenotype (11). In the recombinant line, 97% of alleles tested were homozygous BALB/c.

In order to map the *Axd* mutation, a cross was performed between *Axd* males (on BALB/c background) and C57BL/6 females. Affected heterozygous offspring (recognized by the presence of tail flexion defects) were intercrossed to generate litters in which embryos were isolated at E13.5. The rationale of this approach was that the *Axd* mutation would remain associated with the BALB/c genetic background, and not be replaced by C57BL/6 genomic DNA in affected individuals. Details of the linkage strategy are provided in the Supplementary Material. In summary, genomic DNA from 40 embryos with open spina bifida was pooled and typed by PCR for 105 microsatellite markers that were polymorphic between BALB/c and C57BL/6 and evenly spread over the autosomes (~30 cM intervals). The involvement of the sex chromosomes had previously been excluded (11). In the absence of linkage to a genomic locus, a 1:1 ratio of BALB/c and C57BL/6 alleles would be expected in embryos with spina bifida. Only chromosome 15 showed a divergence from the 1:1

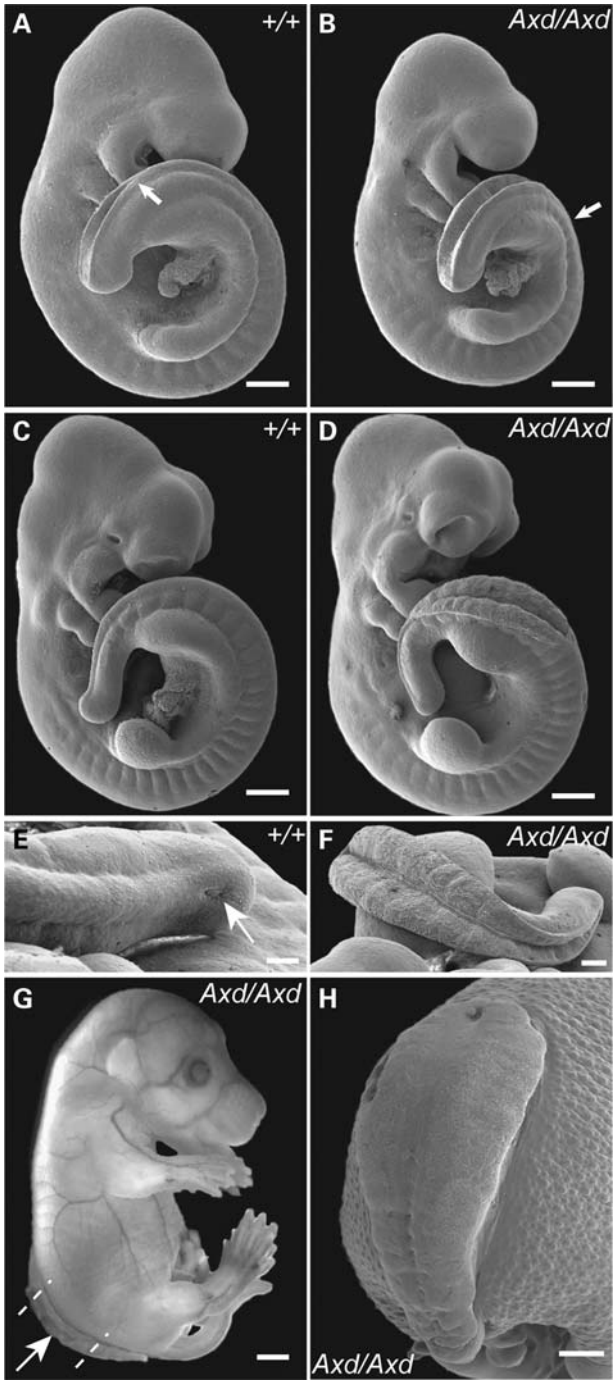

Figure 1. Failure of PNP closure in *Axd* mutant embryos. (**A**, **C** and **E**) Scanning electron microscopy of wild-type embryos reveals that PNP closure has progressed beyond the last formed somite and is at the level of the hindlimb bud at the 24 somite stage (arrow in A); by the 31 somite stage (C and E), the PNP has reduced in size to a small slit (arrow in E). (**B**, **D** and **F**) In contrast, *Axd* mutant embryos exhibit dramatically enlarged PNPs at both 26 and 31 somite stages (B and D, respectively), in which closure does not progress beyond the level of somite 24 (arrow in B). At the 26 somite stage (B), the neural folds of the mutant embryo appear elevated, although closure has not progressed. By the 31 somite stage, the neural folds are splayed wide apart (D and F). (**G** and **H**) In an *Axd* mutant fetus at E16.5, open spina bifida is evident (arrow in G) affecting the low thoracic, lumbar and sacral regions. Transverse sections at the levels indicated by dashed lines in (G) are included in Supplementary Material, Fig. S1. Scale bars: 500 μm (A–D), 100 μm (E), 200 μm (F), 2 mm (G) and 1 mm (H).

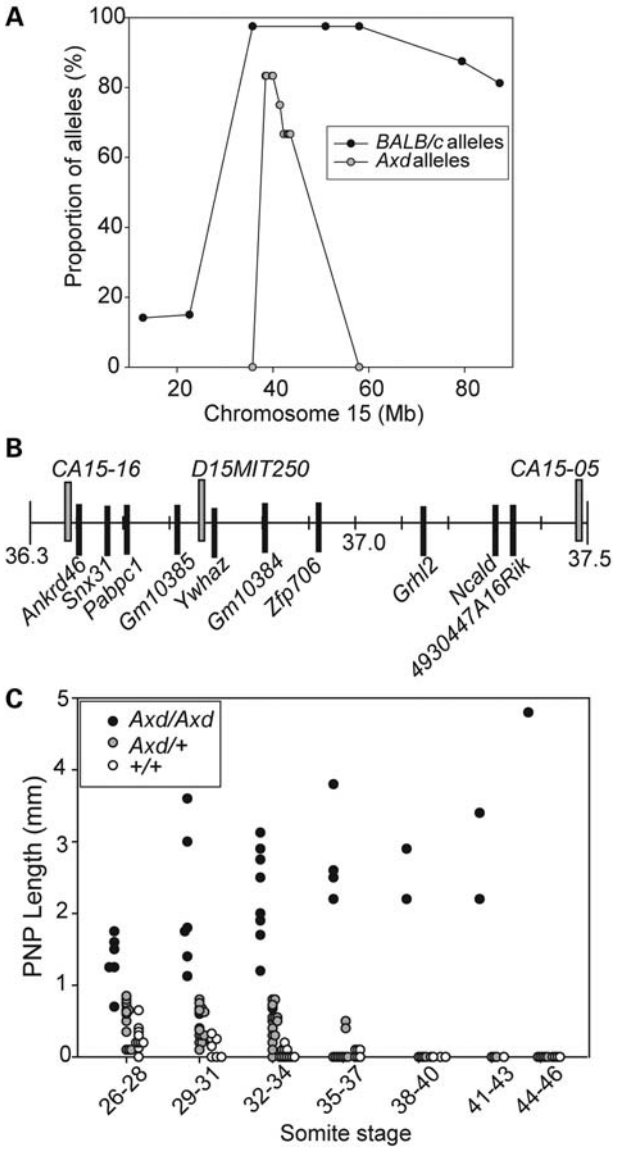

Figure 2. The *Axd* mutation maps to a critical region on mouse chromosome 15. (**A**) In DNA from embryos with spina bifida from an intercross of *Axd* and C57BL/6 mice, typing of polymorphic markers showed a peak of BALB/c and *Axd* alleles (non-C57BL/6) between D15Mit252 and D15Mit171 (22.6–79.4 Mb). Within this region, a peak of *Axd* alleles (non-BALB/c or C57BL/6) was present at 38.5–43.6 Mb. (**B**) Using additional novel polymorphic markers, a critical region of 1.1 Mb was defined between markers CA15–16 and CA15-05 (36.4–37.5 Mb). This region contains 10 known genes (black boxes), as well as 3 RNA genes and various putative processed transcripts (as of Ensembl release 60). The marker D15Mit250 showed 100% association of homozygosity for *Axd* alleles with spina bifida. (**C**) In embryos that were genotyped using D15Mit250, the PNP length was compared at stages during and after spinal neural tube closure. The PNP fails to shorten and close in homozygous *Axd/Axd* embryos (black circles), leading to spina bifida. In contrast, most wild-type embryos exhibit closed PNPs by the 29–31 somite stage (white circles) and *Axd*/+ embryos complete closure by the 35–37 somite stage in most cases (grey circles).

ratio. This apparent association between an *Axd* locus on chromosome 15 and the spina bifida phenotype was further investigated by individual analysis of affected embryos.

The *Axd* critical region was refined using 40 additional informative markers (of 100 tested), which revealed a peak of BALB/

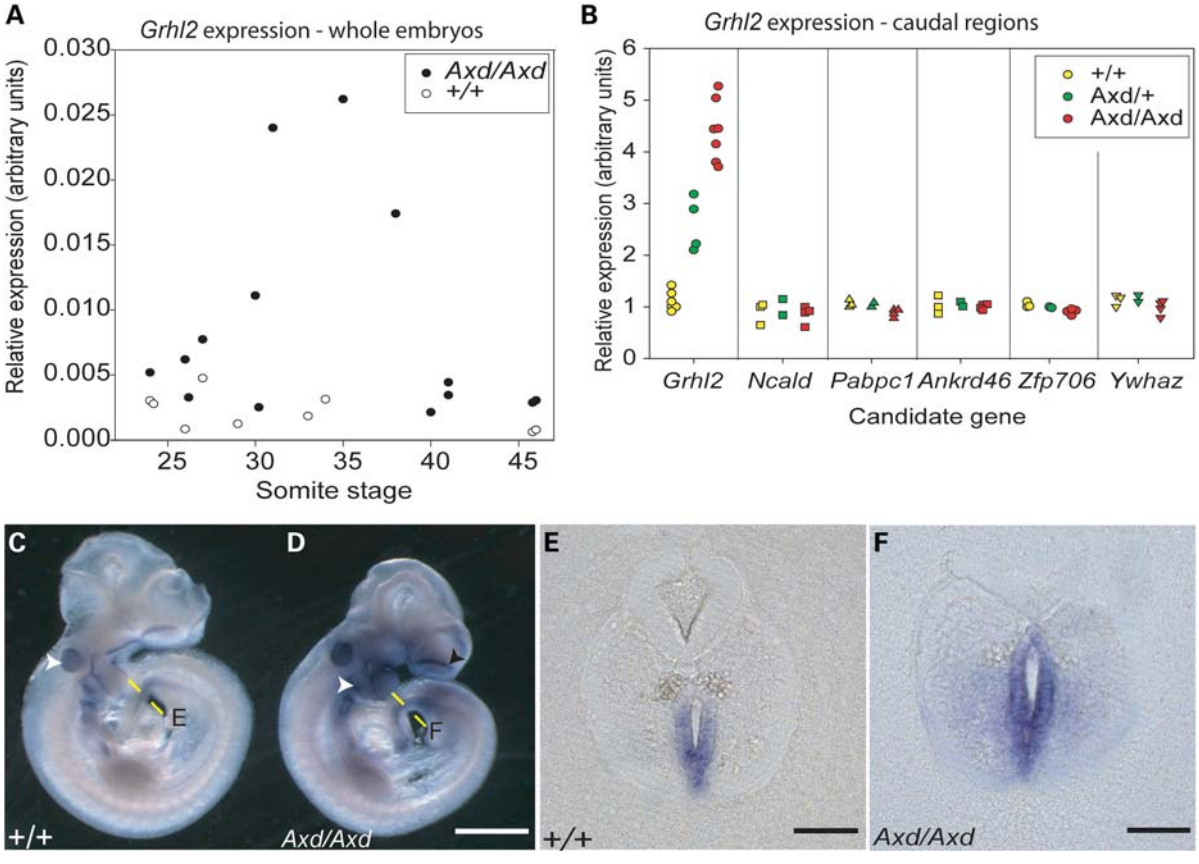

Figure 3. Expression of *Grhl2* is elevated in *Axd* mutant embryos. (**A** and **B**) Expression analysis by qRT–PCR using mRNA extracted from whole embryos (A) and isolated caudal regions (B), at the 30–31 somite stage. There is significant up-regulation of *Grhl2* expression in *Axd/Axd* embryos compared with wild-type littermates, particularly from the 25 somite stage onwards (A). Heterozygous embryos exhibit an intermediate level of *Grhl2* expression in the caudal region (B), whereas no difference in expression was observed for the remaining genes in the *Axd* critical region. (**C**–**F**) Whole-mount *in situ* hybridization for *Grhl2* consistently shows more intense staining in intact *Axd/Axd* embryos (D) compared with wild-type controls (C). Sites of expression include the otic vesicle (white arrowhead in C), pharyngeal region (white arrowhead in D) and forebrain (black arrowhead in D). Sections through the caudal region (at the level of the dotted lines in C and D) reveal expression of *Grhl2* in the hindgut endoderm, whereas the neural folds are negative (E and F). Note the more intense hindgut expression in the *Axd/Axd* embryo (F) with apparent ectopic expression in mesoderm lateral to the hindgut, which is not observed in wild-type (E). Scale bars: 1 mm (C and D) and 0.1 mm (E and F).

c and *Axd* alleles (i.e. absence of C57BL/6 alleles) between D15Mit252 and D15Mit71 (22.6–79.4 Mb). Within a narrower interval (38.5–43.6 Mb), 11 informative markers could discriminate the *Axd* alleles from BALB/c and C57BL/6, confirming association (Fig. 2A). High-resolution mapping, using a combination of additional D15Mit markers, novel polymorphic DNA markers based on nucleotide repeat sequences and an additional cross to C57BL/6 (generating a second recombinant line), further narrowed the critical region to an interval of 1.1 Mb (36.4–37.5 Mb) flanked by heterozygous sequences (Fig. 2B). A 100% association was observed between homozygous *Axd* alleles for D15Mit250 (at 36.7 cM) and the presence of a large PNP ($n > 150$ embryos) in embryos at E10.5 (Fig. 2C). Therefore, in subsequent experiments, this marker was used to genotype embryos from heterozygous *Axd* intercrosses on the BALB/c background.

Grhl2 is over-expressed in Axd mutant embryos

The *Axd* critical region harbours 10 protein-coding genes (Fig. 2B) and three RNA genes (*AC137871.1*, *AC114008.1* and *AC121814.1*) encoding micro-RNA or non-coding RNA, as well as three loci encoding putative processed transcripts (as at Ensembl release 60). The corresponding human syntenic region is at chromosome 8q22. The coding regions and intron–exon boundaries of *Ankrd46*, *Pabpc1*, *Ywhaz*, *Zfp706*, *Grhl2* and *Ncald* were sequenced and no mutations were detected (data not shown). In order to investigate the possibility that a regulatory mutation might result in abnormal expression of one of these *Axd* candidate genes, expression levels were analysed by quantitative real-time RT–PCR (qRT–PCR). A series of embryos at stages during and immediately after spinal neurulation were selected that either displayed a large PNP or spina bifida and genotyped as *Axd/Axd* ($n = 14$) or had a normal or closed PNP and typed as wild-type ($n = 9$). The expression of *Grhl2* showed marked up-regulation in *Axd/Axd* embryos, with an overall expression elevation of ~2.5-fold ($P < 0.001$, Mann–Whitney rank sum test) and a peak at the 30–35 somite stage, when up to 5-fold increase in expression was observed (Fig. 3A). None of the other five candidate genes analysed showed a significant difference in

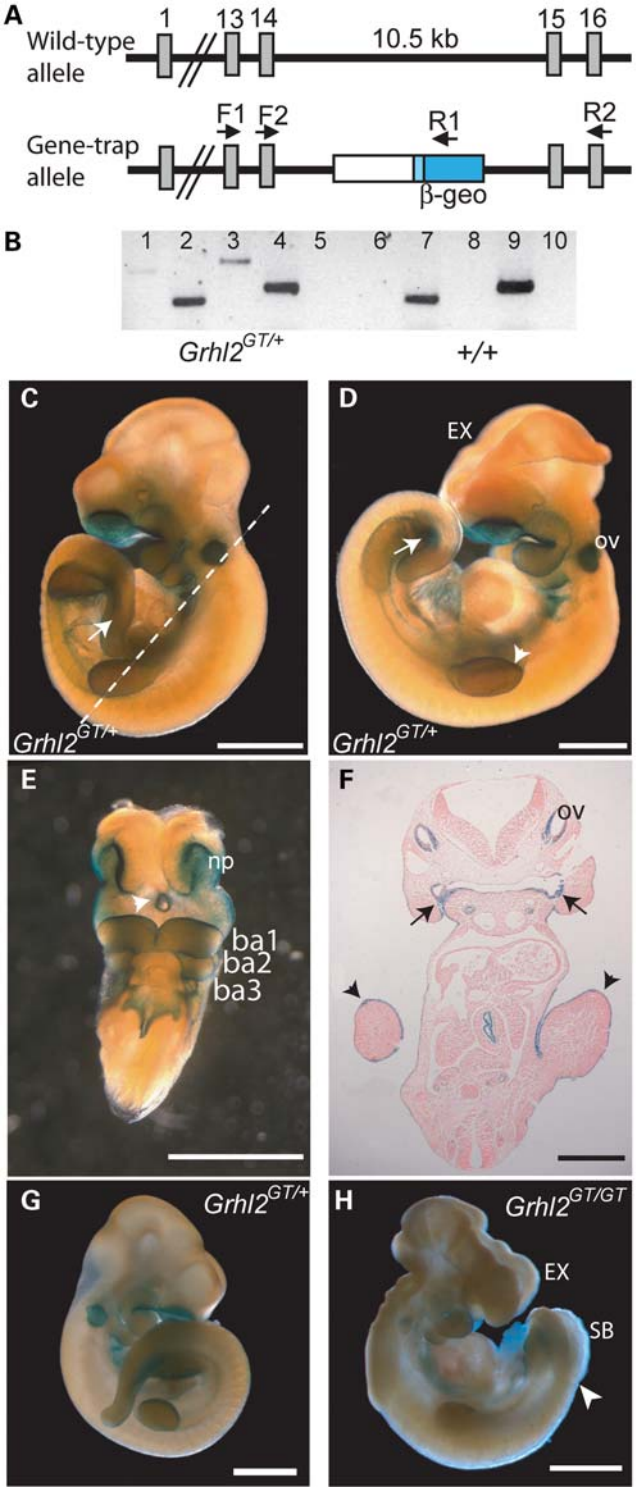

Figure 4. A gene-trap allele of *Grhl2* results in NTDs. (**A**) The gene-trap vector is inserted in intron 14 of the *Grhl2* gene. Schematics of wild-type allele (top) and β-geo-containing gene-trap allele (bottom). F1, F2, R1, R2: PCR primers. Grey bars: exons. (**B**) Efficacy of gene-trapping was confirmed by RT–PCR using cDNA generated from $Grhl2^{GT}$/+ (lanes 1–4) and +/+ (lanes 6–9) embryos (lanes 5 and 10 are no RT controls). Primer pairs that span exons 13–16 (F1 and R2; lanes 4 and 9) or exons 14–16 (F2 and R2; lanes 2 and 7) amplify the wild-type transcript from both +/+ and $Grhl2^{GT}$/+ embryos, whereas the trapped allele (amplified by primer F1 or F2 with R1) was detected only in $Grhl2^{GT}$/+ samples (lanes 1 and 3). (**C**–**F**) X-Gal staining of $Grhl2^{GT}$/+ embryos on the C57BL background, shown in side view (C and D), ventral view (E) and sectioned at the level of the dashed line in (C) (F). Efficacy of gene-trapping is confirmed, as is the *Grhl2* expression pattern which closely resembles that observed by whole-mount *in situ* hybridization (Fig. 3). Note expression in hindgut (arrows in C and D), branchial arches (ba), nasal pit (np) and Rathke's pouch (white arrowhead in E), otic vesicles (ov), foregut (arrows) and ectoderm lining the limb buds (arrowheads in F). In some heterozygous embryos on the C57BL background, we observed exencephaly with 'split face' (EX in D). (**G** and **H**) On the BALB/c background, exencephaly with split face was observed together with spina bifida (SB: neural folds open to the level of arrowhead in H) in homozygous $Grhl2^{GT/GT}$ embryos (H), whereas heterozygotes were usually normal (G). Scale bars: 1 mm in all panels, except (F) (0.5 mm).

expression between mutant and wild-type embryos (Supplementary Material, Fig. S3).

We further analysed mRNA levels in the isolated caudal regions of a separate series of 30–31 somite stage embryos to focus on the embryonic region undergoing spinal neurulation (Fig. 3B). This analysis showed that *Grhl2* expression is significantly elevated, by ~4-fold, in homozygous mutants, while heterozygotes exhibit a level intermediate between +/+ and *Axd/Axd* (Fig. 3B). In contrast, expression of the other genes in the critical region did not vary with genotype. Together, these studies demonstrate that up-regulation of *Grhl2* correlates with failure of PNP closure in *Axd/Axd* embryos. Indeed, this can be visualized by plotting the PNP length against relative expression of *Grhl2* which demonstrates an approximately linear relationship over at least a 5-fold range of *Grhl2* levels (Supplementary Material, Fig. S4). Whole-mount *in situ* hybridization for *Grhl2* showed markedly more intense staining in *Axd/Axd* embryos compared with wild-type or heterozygous littermates (Fig. 3C–F), including in the pharyngeal region, otic vesicles, forebrain and hindgut. Therefore, *Axd/Axd* embryos appear to exhibit an up-regulation of *Grhl2* at all sites of expression.

Grhl2 has close homology and shares a consensus-binding sequence with *Grhl3* (16,17), whose loss of function following gene targeting or down-regulation in the *curly tail* mutant results in spina bifida (13–15). Delayed eyelid closure has been noted in *Grhl3* mutant mice, with closure not completed in any *Grhl3* null fetuses by E16.5 compared with 100% closure in wild-type (18). Similarly, we noted lack of eyelid closure at E16.5 in *Axd/Axd* mutants (seven out of seven; Fig. 1G and Supplementary Material Fig. S2), whereas closure was complete in all wild-type and heterozygous fetuses examined (0 out of 11 with open eyelids).

Generation of a loss of function allele of Grhl2

We hypothesized that *Axd* represents a hypermorphic (over-expressing) allele of *Grhl2* based on linkage analysis, up-regulation of expression at the stage of spinal neurulation and phenotypic similarities to *Grhl3* mutants. We reasoned that if excess expression of *Grhl2* is responsible for NTDs in the *Axd* model, then reduction of expression should normalize spinal neurulation. In order to test this idea genetically, we generated a loss of function allele, using a gene-trap of *Grhl2* (Sanger Institute Gene Trap Resource, cell line AC0205). This allele carries the pGT0Ixr trap vector in intron 14 (Fig. 4A). The $Grhl2^{GT}$ allele, therefore, generates a fusion tran-

script lacking exons 15 and 16, which encode the 59 C-terminal amino acids of the Grhl2 protein (full-length protein is 625 amino acids). The location of the gene-trap vector was determined by PCR using combinations of intronic and vector primers. Sequencing of PCR products showed that the insertion site was at 6611 bp of the 10 515 bp intron 14. Efficacy of gene-trapping was confirmed by RT–PCR and X-Gal staining of embryonic stem cell colonies (not shown) and heterozygous embryos (Fig. 4), exploiting the expression of β-geo from the trapped allele. Staining was evident in several ectodermal locations, mimicking the *Grhl2* expression pattern obtained by *in situ* hybridization. Sites included the surface ectoderm lining the branchial arches and limb buds, oral ectoderm, nasal pits, otic vesicles and Rathke's pouch (Fig. 4C–F; Supplementary Material, Fig. S5).

Among heterozygous *Grhl2*^{GT}/+ embryos analysed at E9.5–10.5, we observed a low frequency of cranial NTDs (15%; 11 out of 75 embryos) that was not observed among wild-type littermates. The cranial NTD phenotype involves failure of closure of the neural folds in the forebrain ('split face') and throughout the midbrain (Fig. 4D). In initial experiments, we did not recover homozygous embryos at stages later than E9.5 from intercrosses of heterozygotes, on a mixed 129/Sv and C57Bl/6 background. However, once the *Grhl2*^{GT} allele was backcrossed onto a *BALB/c* background for two generations (prior to intercross to *Axd*, see below), homozygous mutant (*Grhl2*$^{GT/GT}$) embryos could be recovered at E10.5 and these embryos exhibited not only severe exencephaly with 'split face' but also spina bifida (Fig. 4H). Cranial NTDs occurred with 100% penetrance (17 out of 17 homozygotes at E10.5–11.5), and spina bifida occurred in 88% of homozygotes. These findings suggest a key requirement for *Grhl2* in neural tube closure at both rostral and caudal levels of the body axis. The NTD phenotypes that we observed in *Grhl2*^{GT} mutant embryos resemble those recently reported in *Grhl2* knock-out mice (17), suggesting that the *Grhl2*^{GT} allele corresponds to a loss of function.

Normalization of PNP closure in Axd embryos by loss of Grhl2 function

In order to test the hypothesis that over-expression of *Grhl2* causes spinal NTDs in *Axd* mutant mice, we crossed *Axd*/+ and *Grhl2*^{GT}/+ mice to generate *Axd/Grhl2*^{GT} compound heterozygotes. To provide a quantitative measure of the degree to which spinal neurulation is affected by genotype, the length of the PNP was analysed with respect to developmental stage (Fig. 5A). Spinal neurulation was complete, signified by complete closure of the PNP, in the majority of +/+ and *Grhl2*^{GT}/+ embryos by the 31 somite stage. In contrast, the mean PNP length in *Axd*/+ embryos was significantly larger than in wild-type, with closure not occurring until after the 34 somite stage. The delayed closure of the PNP is likely responsible for the tail flexion defects observed in heterozygous animals. Among *Axd/Grhl2*^{GT} embryos, there was an overall significant reduction in the mean PNP length compared with *Axd*/+ embryos at the 30–31 and 32–34 somite stages (Fig. 5A). Thus, although the presence of the *Grhl2*^{GT} allele did not rescue the *Axd* heterozygous phenotype in every

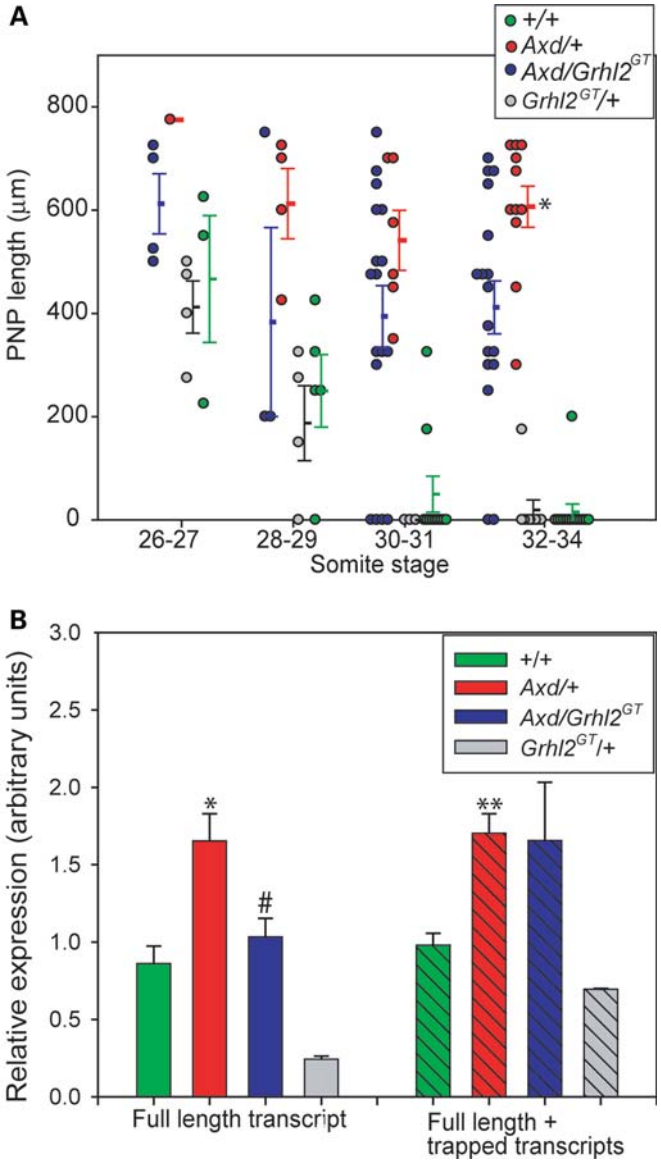

Figure 5. Spinal neural tube closure in *Axd* and *Grhl2*^{GT} compound heterozygotes. (**A**) The length of the PNP (the open region of spinal neural folds) was assessed in relation to developmental stage (as determined by the number of somites) in E10.5 embryos from crosses between *Axd*/+ and *Grhl2*^{GT}/+ mice. Mean PNP length was significantly greater in *Axd*/+ embryos than all other genotypes at the 30–34 somite stages ($^{*}P < 0.001$, one-way ANOVA). *Axd/Grhl2*^{GT} embryos (blue circles) had significantly longer PNPs than *Grhl2*^{GT}/+ (grey circles) or +/+ (green circles) littermates ($P < 0.001$). (**B**) Expression analysis of isolated caudal regions at the 30–32 somite stage, using qRT–PCR. Expression of the full-length *Grhl2* transcript (left side of graph) is greater in *Axd*/+ embryos compared with all other genotypes ($^{*}P < 0.005$, one-way ANOVA). Expression was also elevated in *Axd/Grhl2*^{GT} samples compared with *Grhl2*^{GT}/+ reflecting the functional difference between the wild-type and *Axd* mutant alleles ($^{\#}P < 0.005$). Combined analysis of the full-length and trapped transcripts (right side of graph) shows increased expression in *Axd*/+ samples compared with +/+ or *Grhl2*^{GT}/+ ($^{**}P < 0.05$). *Axd*/+ and *Axd/Grhl2*^{GT} samples do not differ in expression, since the trapped and full-length transcripts are expressed at similar levels.

Axd/Grhl2^{GT} embryo, there was a striking shift towards smaller PNP lengths compared with stage-matched *Axd*/+ embryos. Moreover, 6 out of 35 *Axd/Grhl2*^{GT} embryos had

completed neural tube closure by the 30–34 somite stage, whereas this did not occur in any of the 17 *Axd* /+ embryos examined at these stages. Thus, reduction of *Grhl2* expression level acts to normalize PNP closure in *Axd*/+ embryos.

To evaluate the relationship between *Grhl2* expression level and PNP closure, the caudal region was isolated from a series of embryos and subjected to qRT–PCR for *Grhl2*, using primers (in exons 14 and 16) that amplify the full-length but not the gene-trapped transcript (Fig. 5B). *Grhl2* expression was significantly elevated in *Axd*/+ embryos compared with +/+ embryos, whereas expression in *Axd/Grhl2*^{GT} embryos was comparable with wild-type and significantly lower than in *Axd*/+ embryos. Interestingly, qRT–PCR, using primers in exons 10 and 11, which amplify both the full-length and gene-trapped transcripts, showed that 'total' *Grhl2* expression was comparable in *Axd/Grhl2*^{GT} and *Axd*/+ embryos (Fig. 5B). Thus, normalization of PNP closure correlates with reduction of expression levels of the full-length *Grhl2* transcript, but not the short transcript encoding exons 1–14.

Over-expression of Grhl2 in the hindgut may contribute to increased curvature and altered proliferation in the caudal region

The *Grhl2* expression pattern was determined both by whole-mount *in situ* hybridization (Fig. 3) and by X-Gal staining (Fig. 4). In the caudal region, the site of spinal neurulation, expression was not detected in the neuroepithelium but intense staining was evident ventral to the neural tube. Transverse sections through the caudal region confirmed that this tissue corresponds to the hindgut (Figs 3E and F, and 6A–C). Detection of *Grhl2* in the hindgut at E10.5, but apparently not in the neural folds, is reminiscent of *Grhl3* expression (15) and suggests that failure of neural tube closure in *Axd* mutant embryos results from a defect in a non-neural tissue.

In *curly tail* (*ct/ct*) mice, reduced expression of *Grhl3* in the hindgut results in diminished cellular proliferation and consequently increased ventral curvature that mechanically opposes PNP closure (19,20). The possibility that a similar mechanism might contribute to spinal NTDs in *Axd* mice was raised by the fact that embryos with a large open PNP at E10.5, subsequently genotyped as *Axd/Axd*, were frequently noted to exhibit abnormal ventral curvature of the caudal region (Fig. 6D–E). Measurements of the caudal region in a series of embryos at E10.5 showed that the angle of curvature of the caudal region was indeed significantly greater in *Axd* homozygous mutant embryos than in wild-type or heterozygous littermates (Fig. 6F).

We next investigated whether the increased ventral curvature of *Axd/Axd* embryos could result from a proliferation imbalance in the caudal region, as in *curly tail* mutants. Immunostaining for phospho-histone H3 on transverse sections through the caudal region revealed a significantly lower mitotic index in the hindgut endoderm of *Axd/Axd* compared with wild-type embryos at the 23–28 and 31–33 somite stages (Fig. 6G and H). A small but significant difference in the mitotic index was also noted in the neural folds (Fig. 6G) at the earlier stage but not at the 31–33 somite stage, the stage at which spinal neurulation should be approaching completion (Fig. 6H).

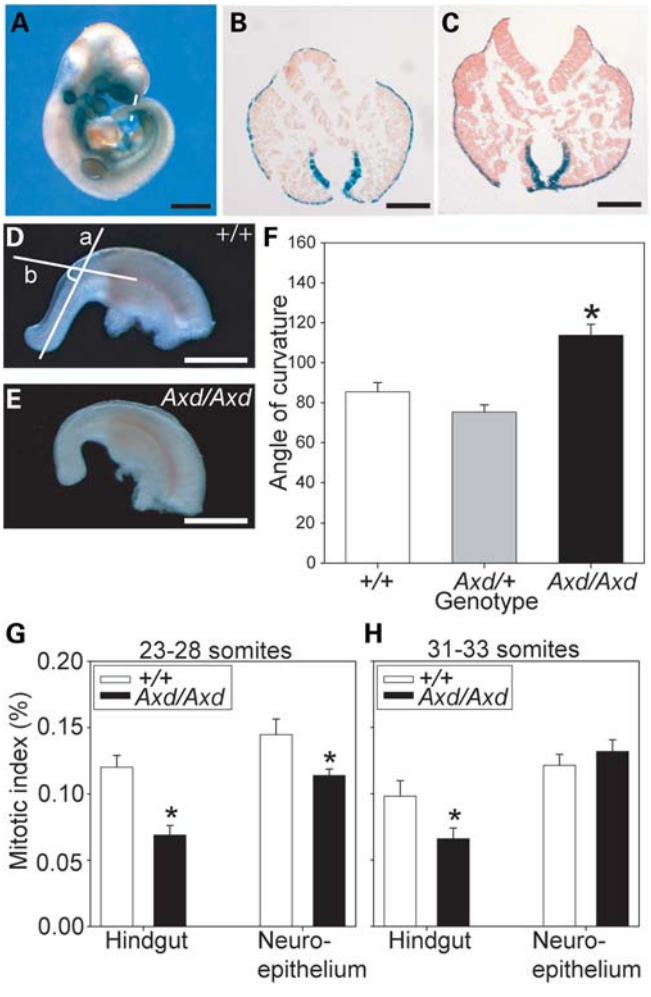

Figure 6. Increased ventral curvature and diminished hindgut cell proliferation in *Axd* mutant embryos. (**A**–**C**) In the caudal region of E10.5 *Grhl2*$^{GT/+}$ (A and B) and *Grhl2*$^{GT/GT}$ (C) embryos, X-Gal staining is detected in the hindgut underlying the PNP region (sections in B and C at the level of the dotted line in A). Note staining also in surface ectoderm. The open neural folds in the *Grhl2*$^{GT/GT}$ embryo (C) correspond to failure of spinal neurulation in this genotype. (**D**–**F**) Ventral curvature of the caudal region appears greater in *Axd/Axd* embryos (E) than in wild-type littermates (D). Quantitation of ventral curvature (angle between lines a and b in A) in a series of 27–33 somite stage embryos at E10.5. *Axd/Axd* embryos ($n = 10$) have significantly greater caudal curvature than either +/+ ($n = 10$) or *Axd*/+ ($n = 18$) littermates ($^*P < 0.001$, one-way ANOVA). Mean somite number did not differ between genotypes (+/+, 31.1 ± 0.5; *Axd*/+, 30.9 ± 0.5; *Axd/Axd,* 30.6 ± 0.6). (**G** and **H**) Mitotic index in the hindgut endoderm and neuroepithelium of E10.5 embryos at 23–28 somite stage (G) and 31–33 somite stage (H). Hindgut proliferation is reduced in *Axd/Axd* embryos compared with +/+ littermates at both stages ($^*P < 0.05$). A smaller but significant difference in mitotic index was also observed in the neuroepithelium at 23–28 somites but not at 31–33 somites. Analysis based on transverse sections at the level of the PNP immunostained for phospho-histone H3. Scale bars: 1 mm in (A), 0.1 mm in (B) and (C) and 0.5 mm in (D) and (E).

Since spinal NTDs occur in association with altered expression of *Grhl* genes in both *curly tail* and *Axd* mutants and have phenotypic similarities, we tested whether the *ct* and *Axd* mutations interact genetically. Homozygous *ct/ct* mice were crossed with *Axd*/+ heterozygotes and the

offspring examined for tail flexion defects. We observed a 2.5-fold increased frequency of curled tails among *ct*/+;*Axd*/+ mice compared with *ct*/+;+/+ ($n = 32$; $P = 0.03$; two-tailed Fisher's exact probability test), suggesting that the *Axd* and *ct* mutations can genetically interact, leading to delay of spinal neural tube closure.

DISCUSSION

The relative paucity of mouse models for isolated spina bifida presents a challenge in identifying candidate genes for the corresponding defects in humans. A parallel hypothesis could be that the genetic aetiology of human spina bifida will prove less complex than anencephaly, in which many more genes are potentially implicated from mouse models.

In the current study, we provide evidence that overexpression of *Grhl2* is the cause of spina bifida in *Axd* mutant mice. Although the *Axd* mutation has not yet been characterized, several lines of evidence support a primary role for *Grhl2* in the *Axd* phenotype. First, *Grhl2* is located in the *Axd* critical region and exhibits misregulated expression in association with failure of spinal neurulation. Second, *Grhl2* is over-expressed in the surface ectoderm and hindgut of *Axd*/*Axd* embryos, both tissues that have been functionally implicated in NTDs in other models (3). Third, we find that loss of function of *Grhl2*, as well as *Grhl3*, causes NTDs, implicating this gene family in neural tube closure (17,21,22). Fourth, *Axd* mutants show eyelid fusion defects reminiscent of those observed in *Grhl3* mutants (18). Finally, delayed closure of the PNP in embryos that are heterozygous for the *Axd* allele can be ameliorated by reduction of *Grhl2* function, following replacement of the wild-type allele with a $Grhl2^{GT}$ allele.

As we could not identify a coding region mutation in *Grhl2* in *Axd* mutants, we carried out additional sequencing of the 5′ and 3′ UTRs including 1.6 kb upstream of the start codon (at chromosome 15: 37 163 142) and a conserved 5′ region (37 111 871–37 112 536). This did not reveal any difference to the mouse genomic sequence database (UCSC Genome Browser). Nevertheless, we hypothesize that the *Axd* phenotype results from a regulatory mutation which leads to increased expression of *Grhl2*. Knock-in of *Grhl2* into the *Grhl3* locus has recently been found to generate embryos with spina bifida which resemble *Grhl3* null mutants (17). This was interpreted to indicate that Grhl2 is unable to compensate for the function of Grhl3 in spinal neural tube closure (17). An alternative explanation, however, is that overexpression of *Grhl2* might have contributed to development of spinal NTDs in these knock-in embryos, as in *Axd*.

Grhl2 functions as a transcription factor (23), and failure of neural tube closure presumably results from misregulation of key downstream genes. The finding of a similar spina bifida phenotype following over-expression or knock-out of *Grhl2* raises questions about the underlying molecular mechanisms and whether the same downstream targets are implicated in each model. In contrast to the spinal neural tube, cranial neurulation appears unaffected by the *Axd* mutation, whereas *Grhl2* null embryos display a severe phenotype with complete absence of closure in fore- and midbrain. This discrepancy could suggest that differing mechanisms underlie NTDs, including spina bifida, in *Axd* and *Grhl2* null embryos. Alternatively, the key *Grhl2* target genes might differ between cranial and spinal regions and those that are essential in the cranial region may be resistant to excessive Grhl2 levels.

Certain features of *Axd* resemble the known pathogenesis in *curly tail* mutant embryos, in which reduced expression of *Grhl3* in the hindgut leads to diminished proliferation and enhanced ventral curvature of the caudal region of the embryo (21). *Grhl2* is also expressed in the hindgut and we find diminished proliferation in this tissue along with increased ventral curvature of the caudal region. We hypothesize that this curvature may contribute to development of spinal NTDs through mechanical inhibition of closure as in *curly tail*. Grhl2 and Grhl3 can form heterodimers as well as homodimers (24), and we speculate that the presence of increased levels of Grhl2 could favour formation of heterodimers in *Axd* mutants at the expense of Grhl3 homodimers. Such an effect could lead to suppression of Grhl3 function, thereby mimicking the *Grhl3* hypomorph, *curly tail*. Indeed, we do observe genetic interaction in double heterozygotes for the *Axd* and *ct* mutations.

Partial penetrance among mouse models of NTDs offers the opportunity to investigate gene–environment interactions and possible prevention of defects by exogenous agents. Spinal NTDs in *curly tail* mice can be partially ameliorated by exposure to retinoic acid, but *in vivo* treatment of *Axd*/+ dams did not alter the frequency of NTDs among litters (25). In contrast, methionine supplementation at neurulation stages, which is ineffective in *curly tail* (26), was found to reduce the frequency of spina bifida in *Axd* litters although a low incidence of exencephaly was also observed (12). A possible association between elevated methionine and cranial NTDs is consistent with findings from embryo culture studies in wild-type mice (27). It will be of interest to determine whether effects of methionine treatment on neural tube closure in *Axd* is associated with alteration in expression of *Grhl2*. For example, reduced expression of *Grhl2* could be associated with normalization of spinal neurulation in *Axd/Axd* embryos but with induction of cranial NTDs in wild-type embryos.

In humans, *GRHL2* has been implicated in age-related hearing impairment (28), with the identification of a *GRHL2* mutation in autosomal dominant non-syndromic hearing loss (29). These conditions are thought to relate to expression of *Grhl2* in the otic vesicle (as we also observe in mice) and the cochlea later in development (29). In the current study, our findings suggest that either loss or gain of function of *Grhl2* can cause spina bifida in the mouse, suggesting a key requirement for regulation of *Grhl2* during spinal neurulation. Moreover, loss of function models demonstrate a critical requirement for *Grhl2* in cranial neural tube closure, including in the forebrain (current study and reference 17). These studies implicate *Grhl2* as a candidate gene for NTDs in humans. It is striking that presumed regulatory mutations affecting expression of both *Grhl2* (*Axd*; current study) and *Grhl3* (*curly tail*; reference 15) have now been found to result in spinal NTDs, perhaps emphasizing the need to consider regulatory as well as missense mutations in searching for the genes contributing to human NTDs.

MATERIALS AND METHODS

Mouse strains

Axd mice were obtained upon rederivation of cryopreserved embryos from Rutgers University, NJ, USA. These mice had a mixed genetic background including the original *Axd* strain (of unknown origin), BALB/c, C57BL/6 and C3H/HeN. Affected heterozygous *Axd* mice were backcrossed multiple times to BALB/c (BALB/cAnNCrl; Charles River) to obtain a congenic strain while monitoring the genetic background using polymorphic microsatellite markers. For linkage analysis, congenic mice were crossed with C57BL/6 (C57BL/6NCrl; Charles River) and then intercrossed to obtain litters which were analysed at E13.5 for the presence of open spina bifida (see Supplementary Materials for details of linkage analysis). Initially, the *Axd* strain (AxBR3) was maintained by a breeding scheme in which heterozygous mice (determined by a curled tail phenotype) were mated with wild-type mice (determined by a lack of phenotype in three subsequent crosses). Following linkage analysis, mice and embryos were genotyped using the D15Mit250 polymorphic marker, which lies between *Pabpc1* and *Ywhaz*.

For generation of mice carrying a gene-trap allele of *Grhl2* (denoted $Grhl2^{GT}$), the AC0205 embryonic stem cell line, carrying the pGT01xr vector inserted in intron 14 of *Grhl2*, was obtained from the International Gene Trap Consortium. Chimeric mice carrying the $Grhl2^{GT}$ allele were generated by blastocyst injection of ES cells (UCL Institute of Child Health ES Cell Facility), and chimeras were mated to C57Bl/6 to test for germline transmission and establish a colony of heterozygous mice. Efficacy of the gene-trap vector and targeting of *Grhl2* were confirmed by X-Gal staining of ES cells and embryos and sequencing of RT–PCR products, generated using a forward primer in exon 14 of *Grhl2*, with a reverse primer in the trap vector (see what follows for RT–PCR details; sequence of primers available on request). The gene-trap vector insertion site was localized in intron 14 using a series of 20 primer pairs designed against the intron in combination with vector-specific primers. This allowed design of a genotyping strategy based on PCR of genomic DNA (see Supplementary Material).

Sequence analysis

Overlapping DNA fragments were amplified by PCR from pools of genomic DNA prepared from three E10.5 embryos with open spina bifida and three wild-type embryos. Primer sequences are available on request. PCR products were purified (GenElute PCR Clean-up Kit, Sigma) and used as template for cycle-sequencing reactions (Applied Biosystems, Big Dye Terminator), which were analysed with an ABI PRISM 3100 Genetic Analyzer (Applied Biosystems).

Collection of embryos and X-Gal staining

Embryos were obtained from timed matings: noon on the day of finding a copulation plug was designated 0.5 days of embryonic development (E0.5). Pregnant females were killed by cervical dislocation and embryos were dissected from the uterus in phosphate buffered saline (PBS) or Dulbecco's modified Eagle's medium containing 10% fetal calf serum. Embryos designated for DNA/RNA isolation were snap-frozen in liquid nitrogen or dry ice and stored at −80°C. Embryos for *in situ* hybridization or histological analysis were washed in diethyl pyrocarbonate (DEPC)-treated PBS and fixed in 4% paraformaldehyde (PFA) in DEPC-PBS at 4°C overnight, or in Bouin's fluid at room temperature for several days.

Embryos for X-Gal staining were fixed in ice-cold 0.2% glutaraldehyde in PBS, rinsed in PBS and incubated in staining solution: 1× PBS, 2 mM $MgCl_2$, 20 mM Tris–HCl (pH 7), 0.2% NP40, 10 mM $K_3Fe(CN)_6$, 10 mM $K_4Fe(CN)_6{\cdot}H_2O$ with X-gal (100 mg/ml in dimethyl sulfoxide) as a 1:50 (v:v) addition at 37°C overnight. Embryos were re-fixed in 4% PFA at 4°C, dehydrated to methanol and stored at −20°C prior to embedding in paraffin wax, sectioning at 5 μm thickness and counter staining with eosin.

Whole-mount *in situ* hybridization and immunohistochemistry

Whole-mount *in situ* hybridization was performed as described previously (15), using a digoxygenin-labelled cRNA probe which was complementary to nucleotides 366–1217 of the *Grhl2* transcript (NM_026496). Embryos were embedded in gelatine-albumin and sectioned at 50 μm thickness on a vibratome, as described previously (30).

Embryos were embedded in paraffin wax and 7 μm transverse sections were immunostained for phospho-histone H3 (Upstate Biotechnology). Sections through the caudal region were matched for axial level using the hindlimb bud as morphological landmark (14). Mitotic index was calculated for neuroepithelium and hindgut in each section based on the number of stained cells expressed as a percentage of the total number of cells (as determined by number of DAPI-stained nuclei), as described previously (15,31).

Scanning electron microscopy

Embryos were fixed in Bodian's fluid [90 ml of ethanol (80%), 5 ml of acetic acid (99%) and 5 ml of formaldehyde (37%)] and prepared for scanning electron microscopy. After ethanol dehydration, they were critical-point-dried using liquid CO_2, attached to aluminium stubs with silver paint, coated with gold/palladium and viewed at 10 kV with a Philips-XL30 scanning electron microscope (SEM).

RNA isolation, cDNA synthesis and real-time qRT–PCR

For analysis of the six candidate genes in the *Axd* critical region, total RNA was isolated from affected (AxBR4CR1F2), wild-type (AxBR3F2) and BALB/c embryos at 25–43 somite stage (E10.5), using TRI Reagent (Invitrogen) and subsequently purified (RNeasy, Qiagen). First-strand cDNA synthesis was performed according to the manufacturer's instructions (iScript cDNA Synthesis Kit, BioRad). Relative expression of candidate genes was analysed by qRT–PCR using an iQ™5 Real-Time PCR Detection System (Bio-Rad) with iQ SYBR Green Supermix (Bio-Rad). Primers, which spanned exons, were designed using Primer Express 1.5 software (ABI) based on the sequence entries in GenBank (Supplementary Material, Table S2).

Cyclophilin, glyceraldehyde 3-phosphate dehydrogenase (Gapdh) and ribosomal RNA 18S (18S) were used as reference genes. Multiple wild-type and affected samples were tested simultaneously. Sample duplicates differing by more than 0.5 in C_t value were excluded. Values were determined using LinRegPCR, analysis of real-time data, version 9.30 beta. Between-session variation was accounted for using the Factor Correction program (32).

For further analysis of *Grhl2* expression in *Axd* and *Axd/Grhl2*^{GT} embryos, RNA was purified from isolated caudal regions (cut at the level of somite 21), genomic DNA removed by DNase I digestion (DNA-free, Ambion) and first-strand cDNA synthesis performed (SuperScript VILO cDNA Synthesis Kit, Invitrogen). qRT–PCR was performed (MESA Blue Mastermix for SYBR Assay, Eurogentec) on a 7500 Fast Real-Time PCR System (Applied Biosystems), with each sample analysed in triplicate. Primers were designed to amplify exons 10–14 and 14–16 of the mouse *Grhl2* cDNA (Supplementary Material, Table S2), and results were normalized to *Gapdh* as previously (15).

SUPPLEMENTARY MATERIAL

Supplementary Material is available at *HMG* online.

ACKNOWLEDGEMENTS

The authors are grateful to Dawn Lau (UCL) for technical assistance and to Peter Gustavsson (Karolinska Institute), Diana Juriloff and Muriel Harris (University of British Columbia) for helpful discussions. Henk Blom, Cees Oudejans, Margot van Eck van der Sluijs-van de Bor and Matthijs Verhage (VU University and VU University Medical Center, Amsterdam) supported and facilitated this work.

Conflict of Interest statement. None declared.

FUNDING

This work was supported by funding from the Medical Research Council (G0802163 to N.D.E.G., A.J.C.); the Wellcome Trust (087525 to A.J.C., N.D.E.G.); and the Netherlands Organisation for Scientific Research (NWO; 916.36.142). Funding to pay the Open Access publication charges for this article was provided by Wellcome Trust.

REFERENCES

1. Copp, A.J., Greene, N.D.E. and Murdoch, J.N. (2003) The genetic basis of mammalian neurulation. *Nat. Rev. Genet.*, **4**, 784–793.
2. Greene, N.D. and Copp, A.J. (2009) Development of the vertebrate central nervous system: formation of the neural tube. *Prenatal Diag.*, **29**, 303–311.
3. Copp, A.J. and Greene, N.D. (2010) Genetics and development of neural tube defects. *J. Pathol.*, **220**, 217–230.
4. Bassuk, A.G. and Kibar, Z. (2009) Genetic basis of neural tube defects. *Semin. Pediatr. Neurol.*, **16**, 101–110.
5. Greene, N.D.E., Stanier, P. and Copp, A.J. (2009) Genetics of human neural tube defects. *Hum. Mol. Genet.*, **18**, R113–R129.
6. Harris, M.J. and Juriloff, D.M. (2007) Mouse mutants with neural tube closure defects and their role in understanding human neural tube defects. *Birth Defects Res. A Clin. Mol. Teratol.*, **79**, 187–210.
7. Harris, M.J. and Juriloff, D.M. (2010) An update to the list of mouse mutants with neural tube closure defects and advances toward a complete genetic perspective of neural tube closure. *Birth Defects Res. A Clin. Mol. Teratol.*, **88**, 653–669.
8. Botto, L.D., Moore, C.A., Khoury, M.J. and Erickson, J.D. (1999) Neural-tube defects. *N. Engl. J. Med.*, **341**, 1509–1519.
9. International Clearinghouse for Birth Defects Surveillance and Research (2007). Annual Report, The International Centre on Birth Defects, Roma, Italy.
10. Copp, A.J., Brook, F.A., Estibeiro, J.P., Shum, A.S.W. and Cockroft, D.L. (1990) The embryonic development of mammalian neural tube defects. *Prog. Neurobiol.*, **35**, 363–403.
11. Essien, F.B., Haviland, M.B. and Naidoff, A.E. (1990) Expression of a new mutation (*Axd*) causing axial defects in mice correlates with maternal phenotype and age. *Teratology*, **42**, 183–194.
12. Essien, F.B. (1992) Maternal methionine supplementation promotes the remediation of axial defects in *Axd* mouse neural tube mutants. *Teratology*, **45**, 205–212.
13. Ting, S.B., Wilanowski, T., Auden, A., Hall, M., Voss, A.K., Thomas, T., Parekh, V., Cunningham, J.M. and Jane, S.M. (2003) Inositol- and folate-resistant neural tube defects in mice lacking the epithelial-specific factor Grhl-3. *Nat. Med.*, **9**, 1513–1519.
14. Yu, Z., Lin, K.K., Bhandari, A., Spencer, J.A., Xu, X., Wang, N., Lu, Z., Gill, G.N., Roop, D.R., Wertz, P. and Andersen, B. (2006) The Grainyhead-like epithelial transactivator Get-1/Grhl3 regulates epidermal terminal differentiation and interacts functionally with LMO4. *Dev. Biol.*, **299**, 122–136.
15. Gustavsson, P., Greene, N.D., Lad, D., Pauws, E., de Castro, S.C., Stanier, P. and Copp, A.J. (2007) Increased expression of Grainyhead-like-3 rescues spina bifida in a folate-resistant mouse model. *Hum. Mol. Genet.*, **16**, 2640–2646.
16. Ting, S.B., Caddy, J., Hislop, N., Wilanowski, T., Auden, A., Zhao, L.L., Ellis, S., Kaur, P., Uchida, Y., Holleran, W.M. *et al.* (2005) A homolog of *Drosophila* grainy head is essential for epidermal integrity in mice. *Science*, **308**, 411–413.
17. Rifat, Y., Parekh, V., Wilanowski, T., Hislop, N.R., Auden, A., Ting, S.B., Cunningham, J.M. and Jane, S.M. (2010) Regional neural tube closure defined by the Grainy head-like transcription factors. *Dev. Biol.*, **345**, 237–245.
18. Yu, Z., Bhandari, A., Mannik, J., Pham, T., Xu, X. and Andersen, B. (2008) Grainyhead-like factor Get1/Grhl3 regulates formation of the epidermal leading edge during eyelid closure. *Dev. Biol.*, **319**, 56–67.
19. Brook, F.A., Shum, A.S.W., Van Straaten, H.W.M. and Copp, A.J. (1991) Curvature of the caudal region is responsible for failure of neural tube closure in the curly tail (ct) mouse embryo. *Development*, **113**, 671–678.
20. Copp, A.J., Brook, F.A. and Roberts, H.J. (1988) A cell-type-specific abnormality of cell proliferation in mutant (curly tail) mouse embryos developing spinal neural tube defects. *Development*, **104**, 285–295.
21. Gustavsson, P., Copp, A.J. and Greene, N.D. (2008) Grainyhead genes and mammalian neural tube closure. *Birth Defects Res. A Clin. Mol. Teratol.*, **82**, 728–735.
22. Werth, M., Walentin, K., Aue, A., Schonheit, J., Wuebken, A., Pode-Shakked, N., Vilianovitch, L., Erdmann, B., Dekel, B., Bader, M. *et al.* (2010) The transcription factor grainyhead-like 2 regulates the molecular composition of the epithelial apical junctional complex. *Development*, **137**, 3835–3845.
23. Wilanowski, T., Tuckfield, A., Cerruti, L., O'Connell, S., Saint, R., Parekh, V., Tao, J., Cunningham, J.M. and Jane, S.M. (2002) A highly conserved novel family of mammalian developmental transcription factors related to *Drosophila* grainyhead. *Mech. Dev.*, **114**, 37–50.
24. Ting, S.B., Wilanowski, T., Cerruti, L., Zhao, L.L., Cunningham, J.M. and Jane, S.M. (2003) The identification and characterization of human Sister-of-Mammalian Grainyhead (SOM) expands the grainyhead-like family of developmental transcription factors. *Biochem. J.*, **370**, 953–962.
25. Haviland, M.B. and Essien, F.B. (1990) Expression of the *Axd* (axial defects) mutation in the mouse is insensitive to retinoic acid at low dose. *J. Exp. Zool.*, **256**, 342–346.
26. Van Straaten, H.W.M., Blom, H., Peeters, M.C.E., Rousseau, A.M.J., Cole, K.J. and Seller, M.J. (1995) Dietary methionine does not reduce penetrance in *curly tail* mice but causes a phenotype-specific decrease in embryonic growth. *J. Nutr.*, **125**, 2733–2740.
27. Dunlevy, L.P.E., Burren, K.A., Chitty, L.S., Copp, A.J. and Greene, N.D.E. (2006) Excess methionine suppresses the methylation cycle

and inhibits neural tube closure in mouse embryos. *FEBS Lett.*, **580**, 2803–2807.
28. Van, L.L., Van, E.E., Fransen, E., Huyghe, J.R., Topsakal, V., Hendrickx, J.J., Hannula, S., Maki-Torkko, E., Jensen, M., Demeester, K. *et al.* (2008) The grainyhead like 2 gene (GRHL2), alias TFCP2L3, is associated with age-related hearing impairment. *Hum. Mol. Genet.*, **17**, 159–169.
29. Peters, L.M., Anderson, D.W., Griffith, A.J., Grundfast, K.M., San Agustin, T.B., Madeo, A.C., Friedman, T.B. and Morell, R.J. (2002) Mutation of a transcription factor, TFCP2L3, causes progressive autosomal dominant hearing loss, DFNA28. *Hum. Mol. Genet.*, **11**, 2877–2885.
30. Ybot-Gonzalez, P., Copp, A.J. and Greene, N.D.E. (2005) Expression pattern of glypican-4 suggests multiple roles during mouse development. *Dev. Dyn.*, **233**, 1013–1017.
31. Massa, V., Savery, D., Ybot-Gonzalez, P., Ferraro, E., Rongvaux, A., Cecconi, F., Flavell, R.A., Greene, N.D.E. and Copp, A.J. (2009) Apoptosis is not required for mammalian neural tube closure. *Proc. Natl Acad. Sci. USA*, **106**, 8233–8238.
32. Ruijter, J.M., Thygesen, H.H., Schoneveld, O.J., Das, A.T., Berkhout, B. and Lamers, W.H. (2006) Factor correction as a tool to eliminate between-session variation in replicate experiments: application to molecular biology and retrovirology. *Retrovirology*, **3**, 2.